Tailoring the Griffiths-like cluster formation in the insulator ferromagnet spin-glass Gd 2 Ni x Co 1 – x Mn O 6 double perovskite

A. Harbi, Y. Le Godec, H. Moutaabbid, S. Benmokhtar, M. Moutaabbid

Tailoring the Griffiths-like cluster formation in insulator ferromagnet spin glass $Gd_2Ni_xCo_{1-x}MnO_6$ double perovskite

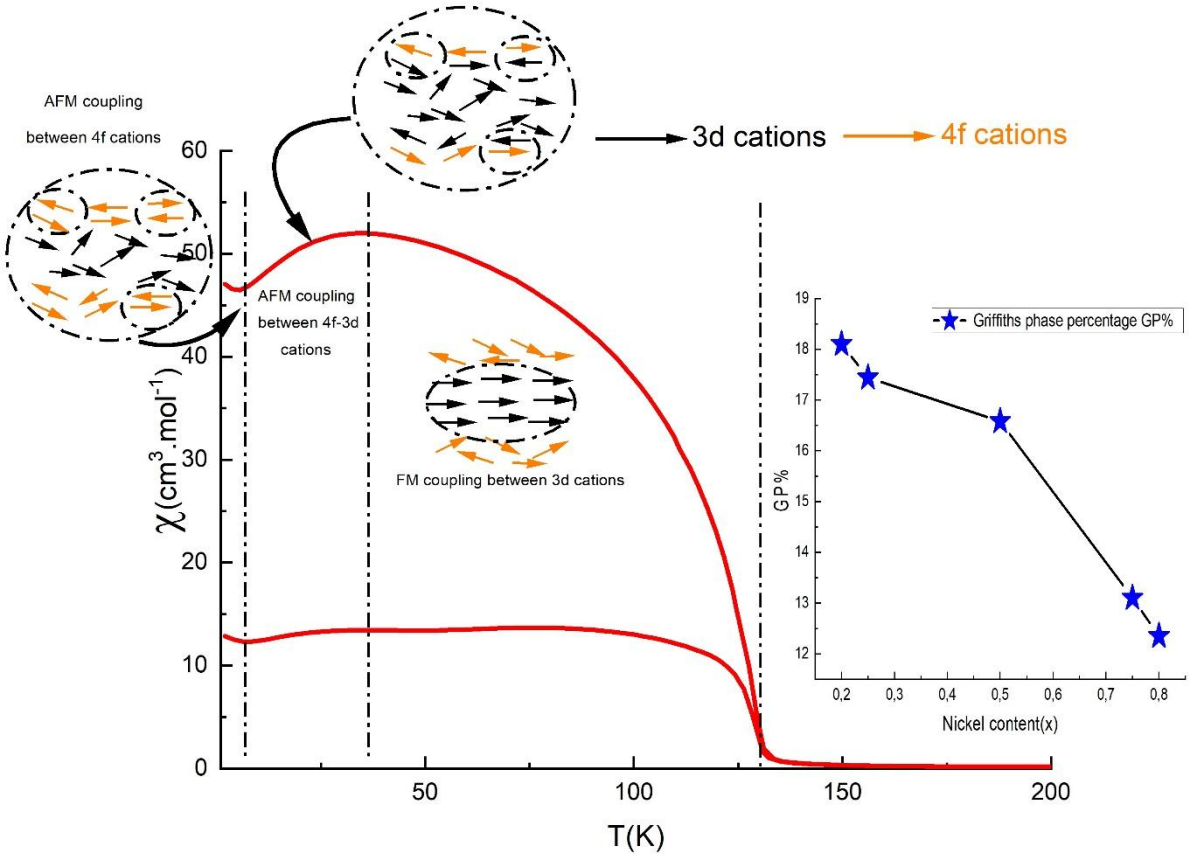

Tailoring the Griffiths-like cluster formation in insulator ferromagnet spin $Gd_2Ni_xCo_{1-x}MnO_6$ double perovskite

A. Harbi[a]*, Y. Le Godec[b], H. Moutaabbid[b], S. Benmokhtar[a], M. Moutaabbid[a]

[a] University of Casablanca, Laboratory of Chemistry and Physics of Materials LCPM, Faculty of Sciences, Department of Chemistry, Casablanca, Morocco.

[b] Institut de Minéralogie et de Physique des Matériaux et Cosmochimie, Sorbonne Université, 4 place Jussieu 75005, Paris, France.

*Corresponding author.

Email: amine.harbi-etu@etu.univh2c.ma

Abstract

In this paper we present the effects of the compositionon structural, vibrational, magnetic, and electronic properties of double perovskite (DP) 3d based manganese oxides $Gd_2Ni_xCo_{1-x}MnO_6$ (GNCMO) powder (for $0 < x < 1$) prepared by high temperature solid state chemistry. These compounds have great research interest due to their specific physical properties.

We have shown that the synthesized compounds exhibit ferromagnetic interaction between the spins of (Mn^{4+}, Co^{2+}), and (Mn^{4+}, Ni^{2+}) cations via oxygen ions and antiferromagnetic interactions between (Gd^{3+}, Co^{2+}), (Gd^{3+}, Ni^{2+}) and (Gd^{3+}, Gd^{3+}) and present a paramagnetic to ferromagnetic phase transition. The paramagnetic Curie-Weiss temperature of GNCMO (T_c) increases from 121K to 128K as the Nickel content increases from 0.2 to 0.8. Further, temperature dependent inverse magnetic susceptibility $\chi(T)^{-1}$ shows deviation from Curie Weiss behaviour around T_G which depicts that Griffiths phase already observed in several perovskite compounds. The value of the GP% percentage and the exponent of ($\lambda < 1$) are found to increase as the Nickel content increases. The hysteresis curve at T = 20K for x = 0.2 displays a meta-magnetic transition explained by the reorientation of the Gd spin moments towards the Mn, Co and Ni spin moments. The imaginary part of susceptibility χ'' showing a small shift of the peak $\sim 1K$ indicating the present of spin or cluster glass behavior.

Keywords: Double perovskites, multiple transition, metamagnetic, Griffiths Phase, spin glass, ferromagnet.

Introduction

In recent years, the magnetic properties of RE_2MMnO_6 (REMMO) double perovskites (RE: rare-earth ions; M: Ni^{2+}, Co^{2+}) has gained much scientific attention with or without others related physical properties, such as giant magnetodielectric properties [1,2] or magnetocalorific effect [3,4]. Like all double perovskites, the magnetic properties of REMMO depend essentially on the crystal structures. This is why a lot of work has been done on the relation-shape between synthesis - structure - magnetic properties [5,6]. Generally, the REMMO perovskite can adopt two different structures, which are the monoclinic structure with $P2_1/n$ space group for ordered state or the orthorhombic *Pbnm* structure for disordered state [7]. The long-range magnetic ordering of Mn^{4+}-O-B^{2+} always display ferromagnetism due to the super-exchange interaction [8]. But the local defects, such as oxygen vacancy [8,9], B-site disordering [10,11] and the antiphase interface between the two FM regions create the antiferromagnetic interactions between the antisite ions Mn^{4+}-O-Mn^{4+} or B^{2+}-O-B^{2+}, that diminishes the long-range FM ordering of Mn^{4+}-O-B^{2+} and weaken the ferromagnetism. The antiferromagnetic interactions could destroy partially the long-range FM interaction and induce the formation of short-range FM, the competition between ferromagnetic and antiferromagnetic interactions in perovskites could results in the frustration of spin ordering, giving rise to spin glass (SG) state or cluster glass (CG) [12].The substitution of R sites by other lanthanides with smaller ionic radii like (Gd, Ho, Er, Tm, Yb) [13-18] involves a significant change in crystalline structure like as the bond length, the angle B-O-Mn, which influences the magnetic properties like as ferromagnetic transition temperature (T_C). While in the specific case of Gd_2BMnO_6 [19-23] the magnetic studies shows a complex magnetic behavior with a multiple magnetic transitions, the long-range magnetic ordering of Mn^{4+}-O-B^{2+} is often the prevailing interaction during the paramagnetic (PM) to ferromagnetic (FM) transitions according to Goodenough-Kanamori rules [24], the antiferromagnetic (AFM) ordering observing below T =50 K attributed to 3d-4f exchange interaction between B and Gd cation and between 4f-4f exchange interaction of Gd cations [19-23]. Therefore, the Curie temperature (Tc) of long-range FM ordering of Mn^{4+} and B^{2+} depends on the B cation nature in the oxides, on the antisite/antiphase percentage and also on the forms of the oxides. Many double perovskite manganites are playground to study inhomogeneous magnetic ground state in the form of clustered or phase separated states. Among the various forms of clustered phases, the “Griffiths like” phase (GP) has drawn more attention due to its interesting magnetic response [25-28]. The Griffiths temperature (TGP) is the characteristic temperature when occurs the formation of the Griffiths phase. For $T_C < T < T_{GP}$, the system is in an unusual magnetic state where the short-range FM clusters of different sizes exist [29-32]. The Griffiths phase has been also reported in some double perovskites

such as Tb_2NiMnO_6 [26], Pr_2CoMnO_6 [13], Ho_2NiMnO_6 [14], Nd_2CoMnO_6 [15] and Lu_2NiMnO_6 [33]. More recently Gd_2CoMnO_6 [34] does not show GP-like behaviour. The tendency to nucleate a Griffiths phase is hence a real challenge to describe and explain the mechanism because it can lead to new technological application not discovered yet except "colossal magnetoresistance" (CMR) in manganites [34].

We address the hitherto unaddressed issue of how the physical properties of the doped double perovskite (GNCMO) from x = 0.2 to 0.8 are correlated to the existence of a Griffiths phase. Therefore, in the present paper, we focus on the properties of the Ni doping on B-site-ordered double perovskite (GNCMO) in order to reveal and explore GP cluster phase in $Gd_2Ni_xCo_{1-x}MnO_6$.

Experimental details

The polycrystalline series of $Gd_2Ni_xCo_{1-x}MnO_6$ (GNCMO) compounds were synthesized using the standard solid-state reaction method. The stoichiometric amounts of powders of Gd_2O_3 (99.9%), NiO (99.9%), $MnCO_3$ (99.9%) and $CoCO_3$ (99.9%) were mixed and calcinated at 1200 °C for 24 h in air with intermediate grinding until the black single phase was prepared. The phase purity and crystal structure of the samples were checked at room temperature by employing the X-ray diffraction technique (XRD), the diffraction data were collected on a Panalytical XPert Pro (θ–θ) diffractometer with Bragg–Brentano geometry using diffracted-beam of CuK_α radiation. The examination of the X ray diffraction data revealed the present of additional peak marked with **(**stars) appears at 2Θ = 28.5° for x = 0.2, 0.75, 0.8 corresponding to Gadolinium oxide (Gd_2O_3) impurities (cubic, $m\overline{3}$ space group, ferromagnetic material). The structural parameters were obtained using the Rietveld structural refinement program implemented in the FULLPROF software suite [35].

The Raman spectroscopy measurements were carried out using HR460 (Jobin-Yvon/Horiba) spectrometer, the laser source used is Ar^+ of the wavelength 514.5 nm.

The optical properties UV-visible spectroscopy measurements were done using Perkin Elmer UV-VIS spectrometer (Lambda 1050).

All direct current (DC) and alternative current (AC) magnetization measurements have been carried out on a Quantum Design MPMS-XL7 magnetometer.

The structural characterization.

The X-ray powder diffraction pattern and the result of the Rietveld refinement for x=0.25 is shown in Figure 1. The crystal structure of $Gd_2Ni_xCo_{1-x}MnO_6$ with x = 0.2, 0.25, 0.5, 0.75 and 0.8 are refined as a monoclinic structure (space group $P2_1/n$), in this model the Cobalt, Nickel (Co^{2+}/Ni^{2+}) and the

Manganese (Mn^{4+}) are placed at wyckoff positions 2b (0, 0, 1/2) and 2a (0, 0, 0) respectively, the gadolinium (Gd^{3+}) and the oxygen (O^{2-}) atoms are placed at different positions 4e (x, y, z), The results of refinement are listed in Table I and are close to the reported values in reference [20]. The composition dependence of the lattice parameters is presented in inset of Figure 1(a) the cell parameters decrease gradually as substituting Ni^{2+} by Co^{2+}, due to the smaller ionic radius of Ni^{2+} (0.69 Å) compared to Co^{2+} (0.74 Å) [36] the same comportment is shown in [37]. The cations Co^{2+}/Ni^{2+} and Mn^{4+} ions are alternately located in octahedral environments linked via O_1 and O_3 along (a, b) axis and via O_2 along c-axis, as shown in inset of Figure 1(b).The bond valence sum was calculated using the relation $V_i = \sum_i \upsilon i$ and $\upsilon_i = \exp \frac{(Ro-R)}{0.37}$ where R is the bond length, the R_0 characterizing the cation–anion distance

(R_0 (Ni^{2+}-O^{2-}) =1.670 Å, R_0 (Co^{2+}-O^{2-}) =1.685 Å and R_0(Mn^{4+}-O^{2-}) =1.750 Å R_0(Gd^{3+}-O^{2-}) =2.148 Å) [38]. The results of calculation show that the Mn atom present in the tetravalent (+4) oxidation state and the Co and Ni atoms are presents in the divalent (+2) oxidation state and Gd is present in the trivalent (+3) oxidation state, these results are consisting with the charge neutrality in GBMO and suggesting the ferromagnetic interaction between the Mn^{4+} and Co^{2+}/Ni^{2+} according to Goodenough-Kanamori rules [24].

The Raman studies.

The dynamical and the structural proprieties of the studied compounds was investigated by the Raman spectroscopy, Figure 2 depicted the obtained results, according to the factor group analysis [39], twenty-four Raman-active modes, represented as ($12A_g$ + $12B_g$) should be present for the monoclinic composition within the system $P2_1/n$. Only seven Raman-active modes can be observed which is lower than the predicted. The spectra display two wide peaks around 620 cm^{-1} and 480 cm^{-1} corresponding to B_g symmetric stretching and to A_g asymmetric stretching modes of Mn-O and Co/Ni-O octahedra while the low frequency vibrations observed between 390 cm^{-1} and 130 cm^{-1} corresponding to the translation of Gd^{3+} cations, as well as a mode of translation and rotation of the octahedra, the same results reported in [22,40]. The composition dependence of the wavenumber of the Raman bands is depicted in inset of Figure 2, we observed the Raman bands shift towards higher wavenumber as the amount of Ni doping increase. The hardening of the phonon may ascribe to the decrease of Ni/Co-O bond length, the same occurs in the case of the double perovskites $La_2Ni_xCo_{1-x}MnO_6$[5].

The electronic structure and optical studies.

The spin-polarized partial density of states (PDOS) and the band structure are carried out using the density functional theory (DFT) based on the spin polarized Kohn-Shame equations with Plane-Wave Self-Consistent Field (PW scf) code implemented in Quantum− ESPRESSO package [41]. In order to find the equilibrium atomic structure, the geometry optimization is performed using Broyden–Fletcher–Goldfarb– Shenno (BFGS) [42] method. The optimization process is stopped when both the maximum force component becomes less than 1 mRy and the stress tensor, expressed as pressure, are less than 0.5 kBar. Table II summarizes the optimized crystal structure parameters against experiment. The obtained lattice parameters values are in good agreement with the experimental values. Figure 3 represent the partial densities of states for x=0.5, the Fermi level is situated at (E_F = 0.0 eV). Using GGA approximation [43] the compounds for x = 0 and 0.5 show a half-metallic character with band gap in the spin-up channel and a continuous band in the spin down channel. The conduction band at the spin-down channel come from the hybridization of O^{2-}, Co^{2+} and /or Ni^{2+} states with bandwidth of 1.072 eV and 4.093 eV. The bands gap at the spin-up channel are expanded in the range -0.21 eV to 0.81 eV and -0.1 to 0.857 eV respectively for x = 0 and x = 0.5. The compound for x = 1 show an insulator behavior both the spin-up and spin-down channels shows a band gap which expands from -0.082 to 1.22 eV and from -0.36 to 0.4 eV. Thus, we introduce a U correction in order to match the experimental data, from the GGA+U calculation with U_{Ni}^{3d}= 5 eV, U_{Mn}^{3d}= 5 eV, U_{Co}^{3d}= 3 eV, U_{Gd}^{4f}= 4.6 eV, all the compounds show an insulator behavior, the spin channels show a band gap. The contributions of PDOS at the valence bands are almost come from O-2p, M-d were (M= Gd^{3+}, Mn^{2+} and Ni^{2+}or Co^{2+}) and Gd-4f states, the overlaps between the orbitals of oxygen and transition metals lead to super-exchange interactions, which is essentially responsible for the nature of the magnetic interactions according to Goodenough–Kanamori rules [24]. On the other side of the Fermi level, the conduction band is mainly consisting of M-3d and Gd-4f states. The GGA+U calculations of band structures Figure 3 gave rise to a ferromagnetic insulator, the minimum of the conduction band and the maximum of the valence band are not at the same point. This indicates that the band gap of all compounds is indirect. The results of the band gap energy using GGA+U approximation are listed in Table III. The experimental bands gap energies for x= 0.5 and x=0.25 were calculated from the UV-Visible absorption spectra in reflection mode using Tauc's formula [44]. The band gap energy value E_g is determined by extrapolating the linear part of the spectrum $(\alpha h\nu)^2$ curve towards the (hv) axis Figure 4. The results show an insulating behavior, the value of the gap energy increases as the Mn-O-B angle decreases for $Gd_2Ni_{0.25}Co_{0.75}MnO_6$ (E_g = 1.92 eV; Mn-O-B = 145.32), for $Gd_2Ni_{0.5}Co_{0.5}MnO_6$ (E_g = 1.88 eV; Mn-O-B = 145.82), and for Gd_2NiMnO_6 (E_g = 1.59 eV; Mn-O-B = 146.2)[22]. These results are confirmed by the theoretical studies on Re_2CoMnO_6 compounds [45], the authors show that the exchange angle θ of the Mn-O-Co bond is an important factor which

influences the degree of overlap between the orbitals of the valence and conduction bands. Therefore, the exchange angle θ decreases, leading to a weaker overlapping of orbitals and a larger band gap.

The magnetic studies.

Figure 5 display the temperature dependent the susceptibility per formula unit (f.u.) in the temperature range of 2K-300K under 50 Oe magnetic field (a), the first derivative of ZFC susceptibility versus temperature between 60K-160K (b). All samples exhibit a ferromagnetic–paramagnetic transition occurring at the Curie temperature (T_{C1}). The ferromagnetic ordering attributed to super-exchange interaction between empty and half-filled e_g orbitals of Mn^{4+}($t_{2g}^3\ e_g^0$) and Co^{2+} ($t_{2g}^5 e_g^2$) or Ni^{2+} ($t_{2g}^6 e_g^2$) via oxygen O^{2-} following the Goodenough-Kanamori rules [24]. The values of the Curie temperature listed in Table IV, T_{C1} increases from 121.9 K to 128.6 K when the content x increases inset of Figure 5, that is predicted as the values of T_{C1} for GCMO varied from 112K to 117.3K for a polycrystalline sample and 112K for a single crystal according to the literature [19-21]. Whereas the values of T_{C1} for GNMO varied from 125K to 130K for a polycrystalline according to the literature [22, 23]. Moreover, the values of the T_{C1} depend also the cation ordering the high Tc reflect a high degree of cation ordering [5,22]. The evolution of dχ/dT versus temperature (T) show also another minima T_{C2} for x = 0.5, 0.8 corresponding to a weak PM-FM transition attributed to the short-range magnetic ordering of Mn^{4+}- O - Ni^{2+} /Co^{2+}. The magnetization curves χ_{FC}(T) increases with decreasing temperature from ~130K to ~50K and then starts to decrease with a broad peak noticed at ~40 K, the downturn behavior reflects the presence of antiferromagnetic interactions between the cations (Co^{2+}, Gd^{3+}), (Ni^{2+}, Gd^{3+}) and (Mn^{4+}, Gd^{3+}) and the Neel temperature T_N corresponds to the maximum value of the broad peak. The similar behavior has been observed in other perovskite as Gd_2CoMnO_6, Gd_2NiMnO_6 with transition temperatures at T_N ~ 47 K [18], T_N ~ 33 K [46] and T_N ~ 49 K [19]. The evolution of the Neel-temperature (T_N) versus temperature (T) is reported in inset of Figure 5. The values of T_N decreases from 48.19 K to 36.18 K when the Nickel content x increases. This is due to an increase in the number of antiferromagnetic interactions of (Co^{2+}, Gd^{3+}), (Ni^{2+}, Gd^{3+}), and (Mn^{4+}, Gd^{3+}) in compounds with low Nickel content. The magnetic moments of the rare earth ions are visible in a low temperature region, while the increase in magnetization observed below 5K corresponds to the short-range antiferromagnetic interaction of the Gd^{3+} cations [19-23]. The curves of the inverse of magnetic susceptibility as a function of temperature χ^{-1}(T) are shown in the Figure 6 for x=0.5, the χ^{-1}(T) starts to deviate from the linear Curie-Weiss behaviour just below T_{GP} = 150 K and shows a

downward curvature and follows a power-law behaviour $\chi^{-1}(T) = A(T - T_C^R)^{1-\lambda}$ where T_C^R is the critical temperature below which χ diverges and λ is an exponent such that $0 < \lambda < 1$ for $T_C^R < T < T_{GP}$ and $\lambda = 0$ for $T > T_{GP}$, the downturn in $\chi^{-1}(T)$ gradually suppresses with increasing field strength and eventually disappears [25, 28]. The same behavior has already observed for a polycrystalline Ho_2NiMnO_6 [13], La_2CrMnO_6[47] and $La_{2-x}Sr_xCoMnO_6$[48] Gd_2CoMnO_6 and Gd_2NiMnO_6 [19-23] and is usually related to the contribution of the both rare-earth (Gd^{3+}) and transition metal ion (Co^{2+}/Ni^{2+} and Mn^{4+}) sublattices or the existence of Griffith Phase (GP) [30,31] due to the presence of higher degree of disorder in polycrystalline sample leading to formation of a short-range ferromagnetic interaction at temperatures above T_C. The calculated values of λ are listed in Table IV and are comparable to those values obtained for different oxides [30, 31] in the region $T_C^R < T < T_{GP}$ and close to zero in the region $T > T_G$. The strength of the GP and the value of λ depend strongly on cation disorder [48]. For example, P R Mandal et al has studied the effect of cation disorder on the structural and magnetic properties in hole doped double perovskite $La_{2-x}Sr_xCoMnO_6$ (x = 0.0, 0.5, and 1), they found that the values of the disorder increase as GP% and λ increases, the lowly ordered of La_2CoMnO_6 has a value of GP% = 15 and a value of λ = 0.83 whereas the highly ordered of $LaSrCoMnO_6$ has a value of GP% = 6 and a value of λ = 0.7. The percentage of GP can be calculated by the following equation $GP(\%T_C) = [\Delta T/T_C] \times 100$ where $\Delta T = T_G - T_C$ (see Table IV), the results show that high Nickel content compounds for x = 0.75 and 0.8 have a low percentage of GP (GP% = 13.1, GP% = 12.35) and consequently a high degree of ordering. However, the compounds for x = 0.2 and 0.25 have a high percentage of GP (GP% = 18.1, GP% = 17.44) and a low degree of ordering. As intended the values of λ increase as the Ni content decrease Figure 7. The total susceptibility was also fitted using the modified Curie Wiess [49] $\chi(T) = \frac{C_{3d}}{T-\theta_{CW}} + \frac{C_{4f}}{T}$ where C_{4f} and C_{3d} are the curie constant of the rare-earth 4f and transition metal 3d ions and Θ_{CW} is the Curie Wiess temperature for the transition metal. The results of the fit according to equation have been listed in Table IV, the obtained values of the curie constant of the rare-earth C_{4f} are higher than the theorical value of C_{Gd}= 15.8 emu $mole^{-1}$ K^{-1} with Lande factor g = 2 [50], and the reported value [17].

Figure 8 present the isothermal field dependent the magnetization for $Gd_2Ni_xCo_{1-x}MnO_6$ at 43K, (a) display the entire M-H loops from -4T to 4T and (b) display the zoomed loops from -1T to 1T without first magnetizations, the saturation has not been attained for any of the samples. The M(H) loops revel two magnetic interactions, the ferromagnetic interactions between the cations (Mn^{4+}, Co^{2+}) and (Mn^{4+}, Ni^{2+}) characterized by irreversible magnetization behavior at low fields (less than 2T) and antiferromagnetic interactions between the cations (Co^{2+}, Gd^{3+}), (Ni^{2+}, Gd^{3+}) and (Mn^{4+}, Gd^{3+}) and between cations (Gd^{3+}, Gd^{3+}) characterized by an almost linear variation of magnetization at high fields (greater than 2T) leading to incomplete saturation of the cycles. The saturation magnetization

(M_S) at 4T extracted from M(1/H) extrapolated to 1/H = 0, the coercive magnetic field (H_C) and the specific remnant magnetization (M_r) are listed in Table IV. The parameters of the hysteresis cycle are extremely dependent on the cationic disorder [5,51] the cationic disorder increases when the M_S decrease and the coercive field and the specific remnant magnetization (M_r) increases. The theoretical saturation moments (Ms_0) calculated using the following equation $Ms_0 = \sqrt{(1-x)\,M^2_{S.GCMO} + x\,M^2_{S.GNMO}}$ .The calculated Ms_0 value are lower than Ms_{ext} this discrepancy explain by the presence of local disorders, such the antisite ions, the anti-phases, the B-site disordering and the oxygen vacancy [8, 11], which diminish the long-range FM ordering of Mn^{4+}-O-B^{2+} the degree of the cation ordering are calculated by the ratio Ms_{ext} /Ms_0, The results show that the compounds with a high nickel content have a high cationic order (>57%) while the compounds with x = 0.2 and 0.25 have a low cationic order. The higher values of Mr and HC in x = 0.2 and 0.5 compared to x = 0.75 and 0.8 may be associated with the large crystalline disorder. Inset of Figure 8 shows M(H) loops at 300 K, the M plotted versus H are straight lines for all compounds indicating the total absence of magnetic coupling between cations at T = 300 K (the paramagnetic range). Field dependent magnetization M(H) measurements performed at 5, 20 and 80K for x = 0.2 and are plotted in Figure 9. The maximum moment value at 5K was 10 µB/f.u. which is very lower than the expected value of M_S = 19.8 µB/f.u, the presence of the antiferromagnetic interactions between the Ni^{2+}/Co^{2+}-O-Mn^{4+} sublattice and the Gd spins can be induced to an incomplete saturation of the hysteresis loops[12, 14, 17]. The evolution of M_S (defined as maximum moment value at 5, 20 and 80K) versus temperature (T) are represented in inset of Figure 9(a) the value of M_s become important at temperatures below to 10K owing to the large contribution of Gd spins leading to incomplete saturation of the hysteresis cycles a such magnetic behavior is also observed in Gd_2CoMnO_6 [43]. The M(H) loops in the temperature 80 K start to saturate and we observe a decreasing in the slope of the linear part of the hysteresis cycle. The derivative of dM/dH at 20K is plotted in inset of Figure 9(b) which shows discontinuities curve at H= -4030 Oe and H= -1017 Oe indicating the presence of metamagnetic transitions, this result is in good agreement with the result of study carried out by Murthy et al [52] on the compound Gd_2CoMnO_6 and on $TbCo_{0.5}Mn_{0.5}O_{3.06}$ [53]. Metamagnetic transitions is described as the transition from an antiferromagnetic spin configuration to a ferromagnetic spin configuration obtained by a variation of temperature or by the application of an external magnetic field. The temperature dependent in-phase χ' component and out phase χ'' component of *AC* molar for x = 0.5 and x = 0.75 with an *AC* field of 3Oe at three frequencies (50Hz, 141.2Hz, 400.6Hz) display in Figure 10. Only one peak has been observed in both χ'(T) and χ''(T) in the temperature range 60-160K, the real part of susceptibility χ' showing the frequencies independent peaks and reveal only PM-FM transitions while the imaginary part of susceptibility χ''

showing a small shift of the peak $\sim 1K$ when the value of the frequencies decreases suggesting the presence of spin glass or cluster glass behavior, the same results are reported in and explained by the presence of structural defects which destroys the magnetic order [5].

Conclusion

In summary, the effects of chemical composition on structural, magnetic, vibrational and electronic properties of double perovskite RE_2NiMnO_6 oxides have been systematically studied in order to better understand the formation of GP cluster in competition with the spin / cluster glass mechanism. The magnetic properties have been investigated by ZFC-FC measurements from 5 K to 300 K the results showing a multiple magnetic interaction, the ferromagnetic interaction between the spins of (3d-3d) cations via oxygen ions and antiferromagnetic interactions between (4f-3d) and (4f-4f) cations. The deviation of inverse susceptibility from Curie-Weiss behavior with $\lambda \leq 1$, indicates a development of the Griffiths phase. The GP% phase and λ parameters are decreasing with the chemical composition. Thus. Spin/cluster glass has been evidenced and is concomitant to GP cluster formation in $Gd_2Ni_xCo_{1-x}MnO_6$. Understanding this mechanism is the first step of new physical application for manganese oxide DP. The tendency to nucleate a Griffiths phase will need further study, especially on its extreme sensitivity to magnetic field.

Acknowledgement

The authors would like to thanks Michel Fialin (Service Camparis, Sorbonne University), Yanling Li (Institut Parisien de Chimie Moléculaire, Sorbonne University), Maxime Guillaumet (IMPMC, Sorbonne University).

Figures

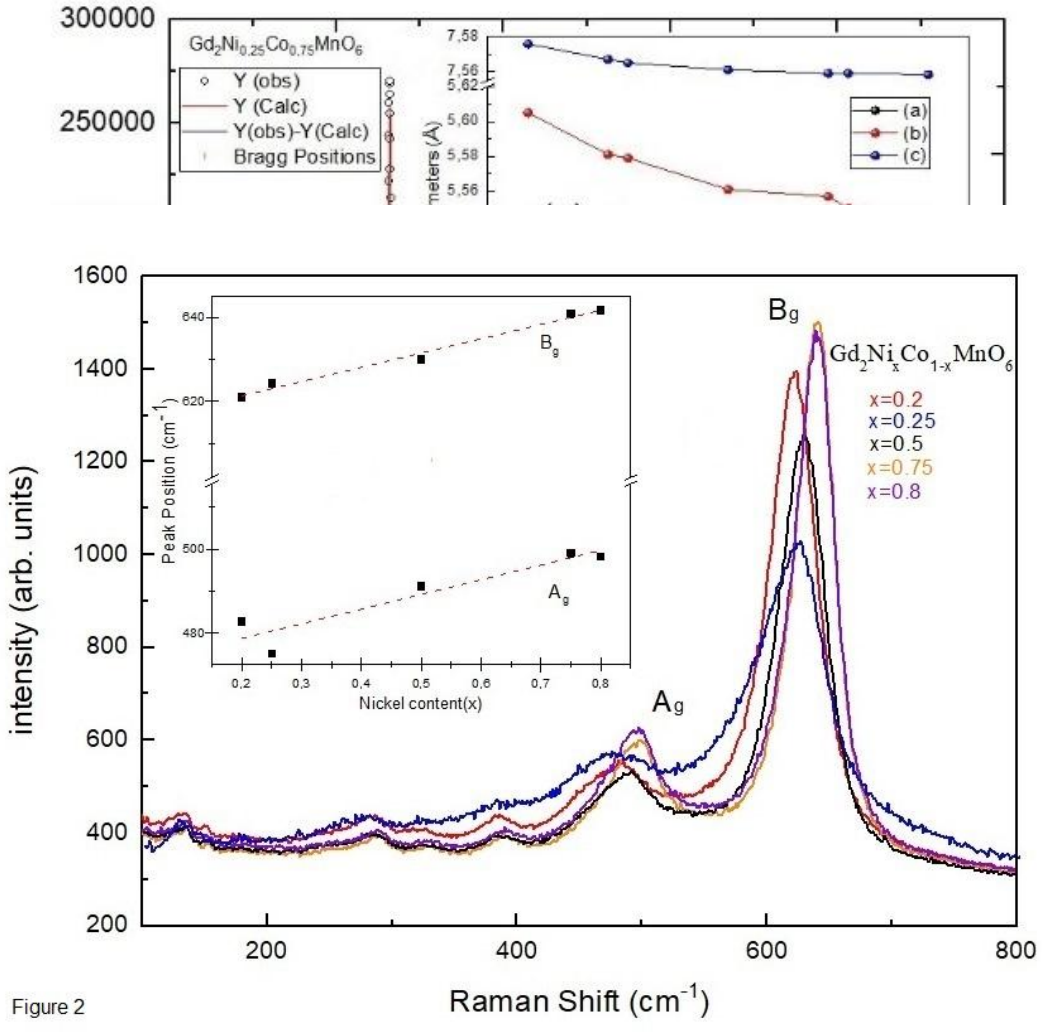

Figure 2

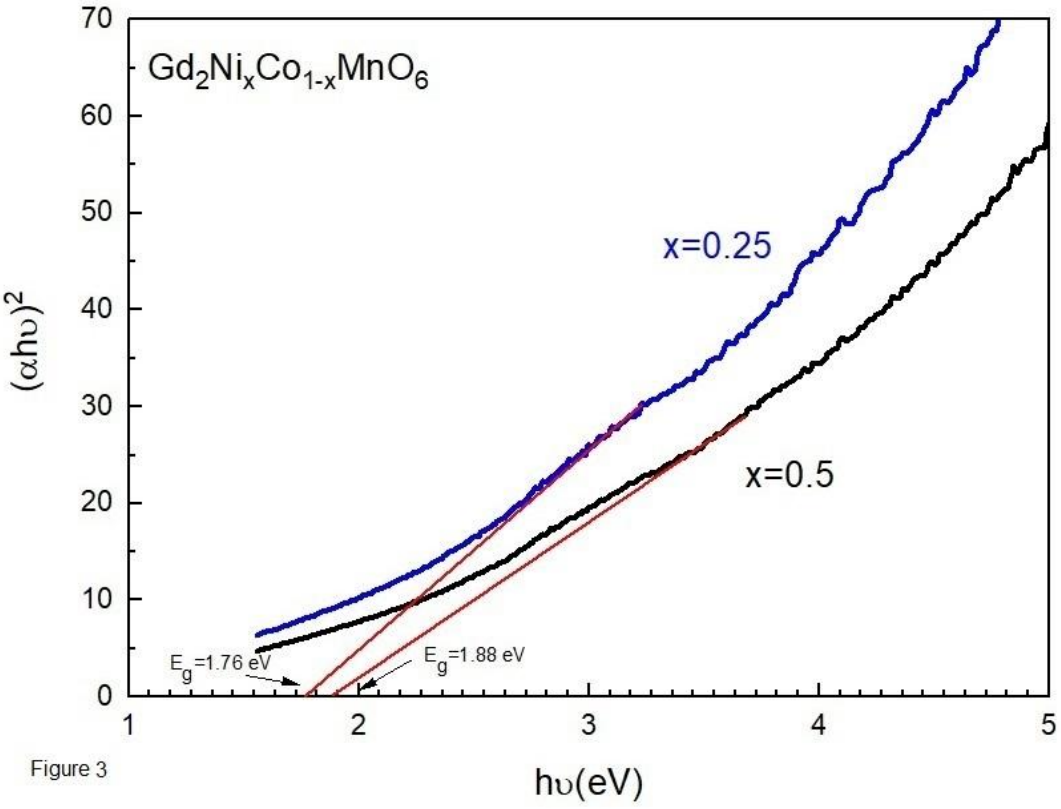
Gd2NixCo1-xMnO6
x=0.25
x=0.5
Eg=1.76 eV
Eg=1.88 eV
(αhυ)2
hυ(eV)
0
10
20
30
40
50
60
70
1
2
3
4
5

Figure 3

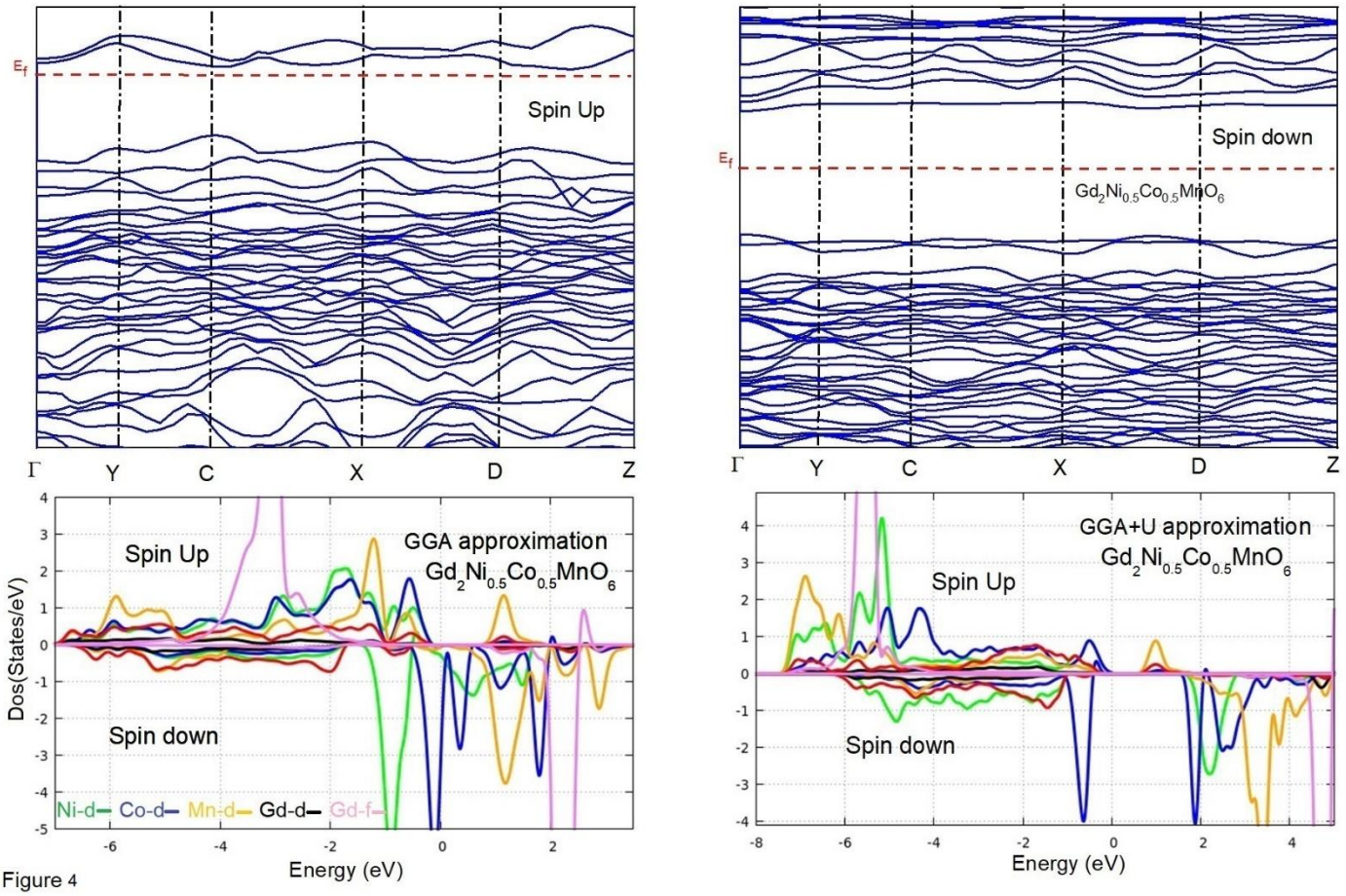
E_f
Spin Up
Γ Y C X D Z
E_f
Spin down
Gd2Ni0.5Co0.5MnO6
Γ Y C X D Z
Spin Up
GGA approximation
Gd2Ni0.5Co0.5MnO6
Spin down
Ni-d Co-d Mn-d Gd-d Gd-f
Dos(States/eV)
Energy (eV)
GGA+U approximation
Gd2Ni0.5Co0.5MnO6
Spin Up
Spin down
Energy (eV)

Figure 4

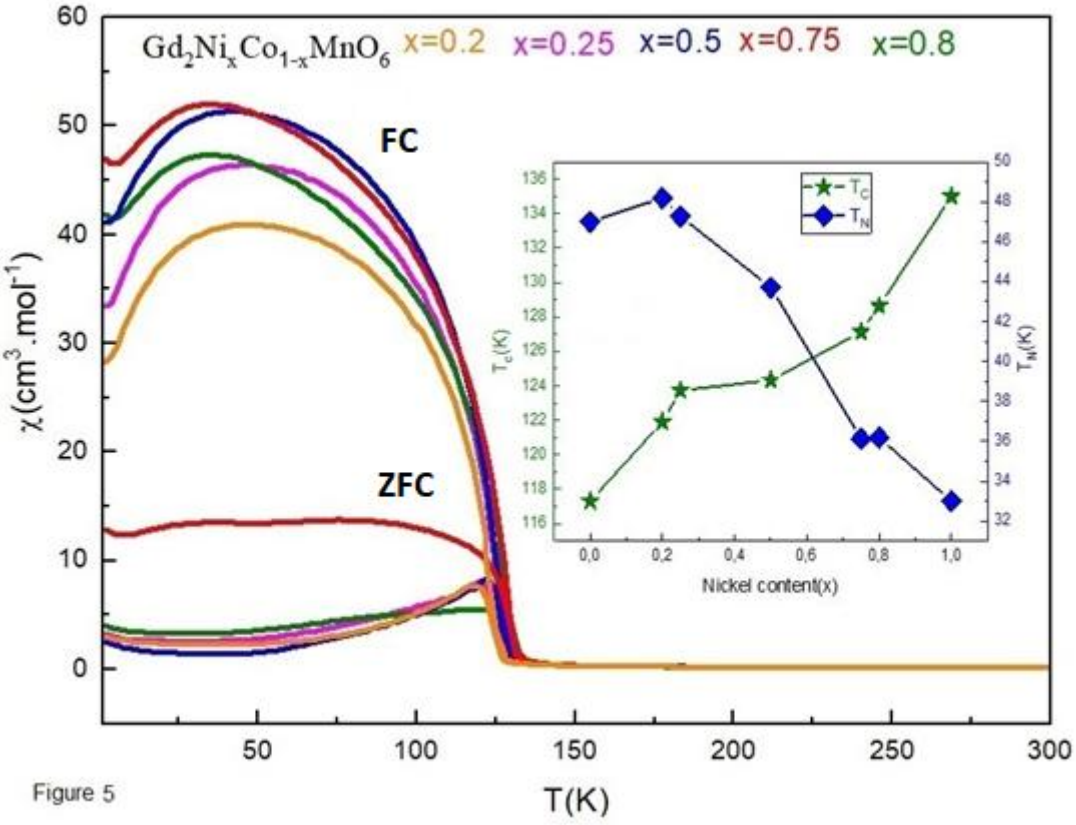

Figure 5

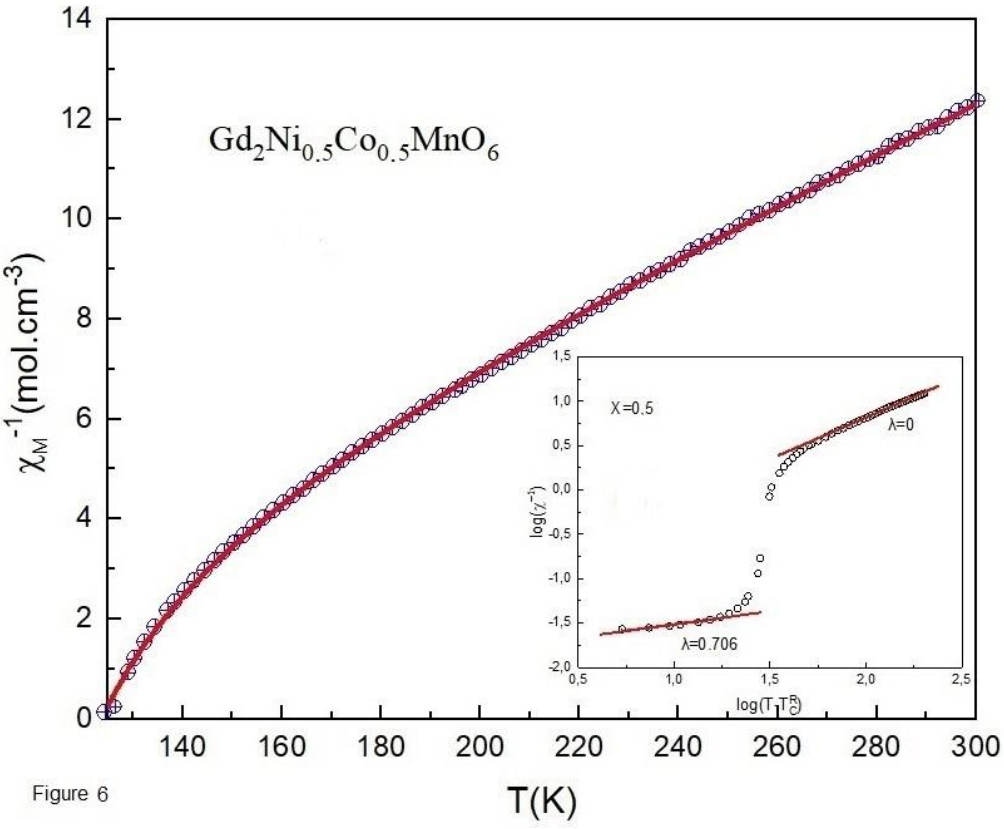

Figure 6

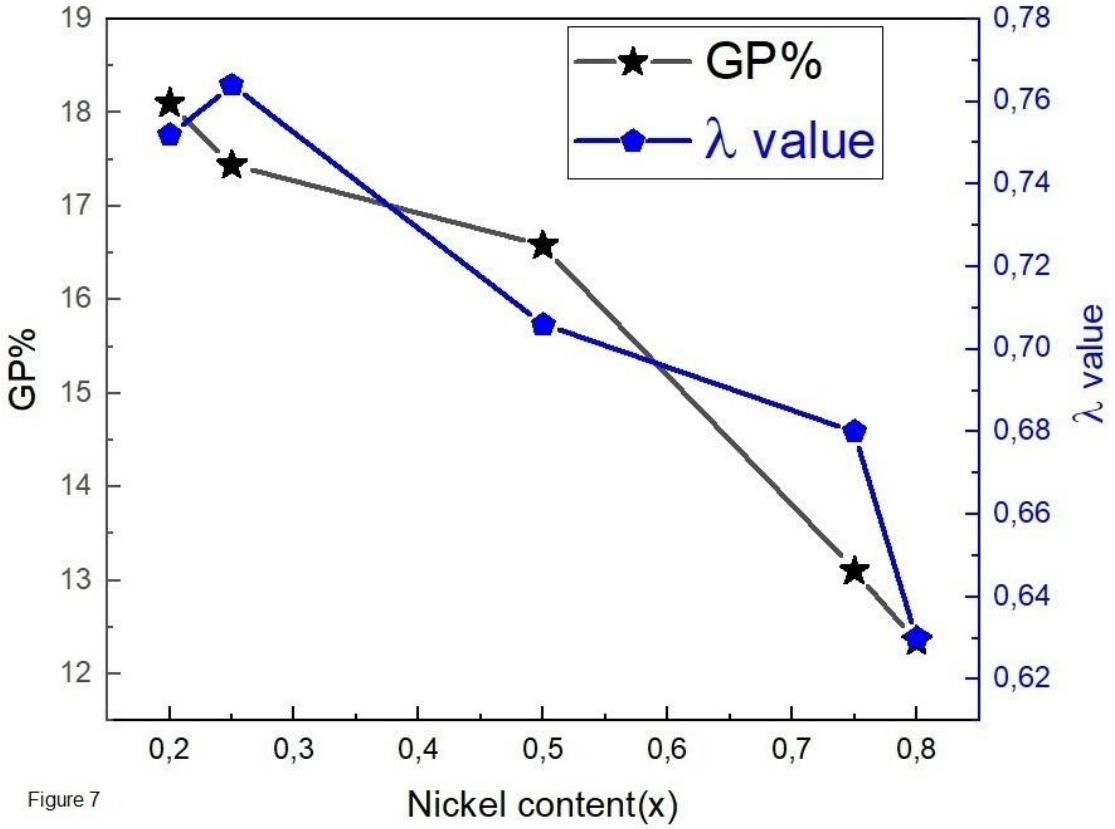

Figure 7

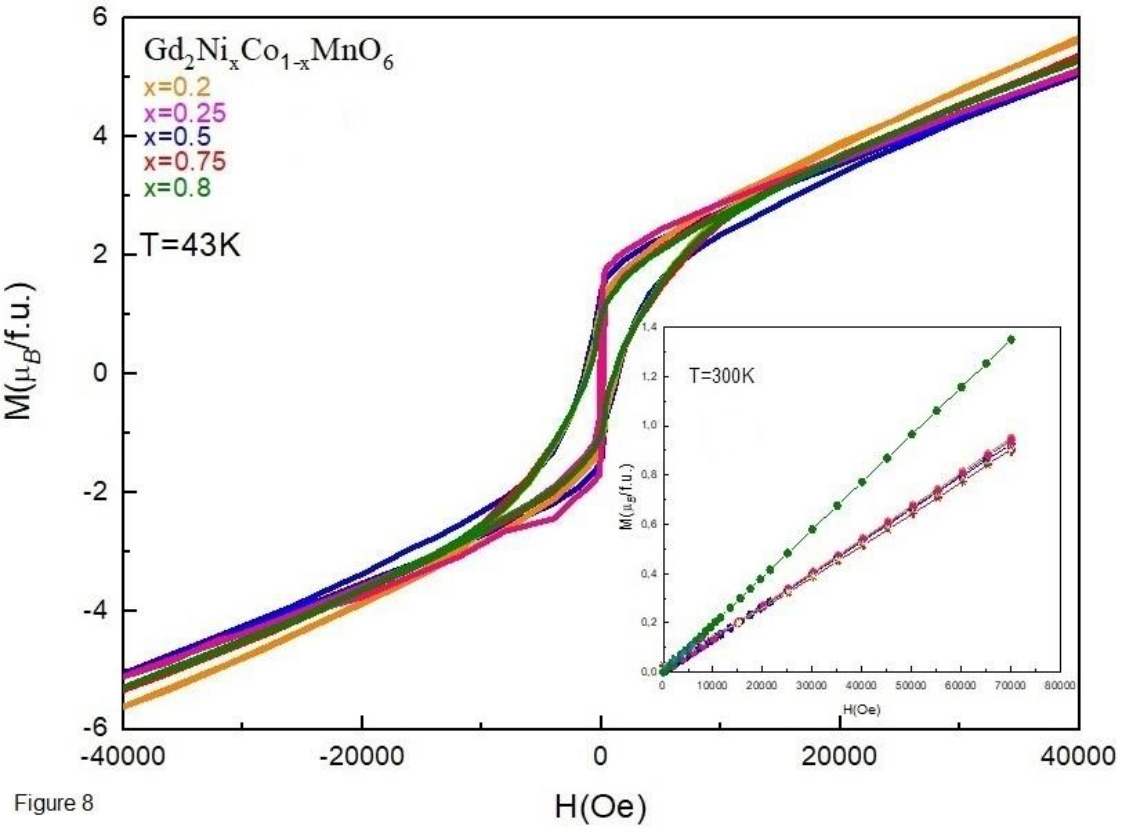

Figure 8

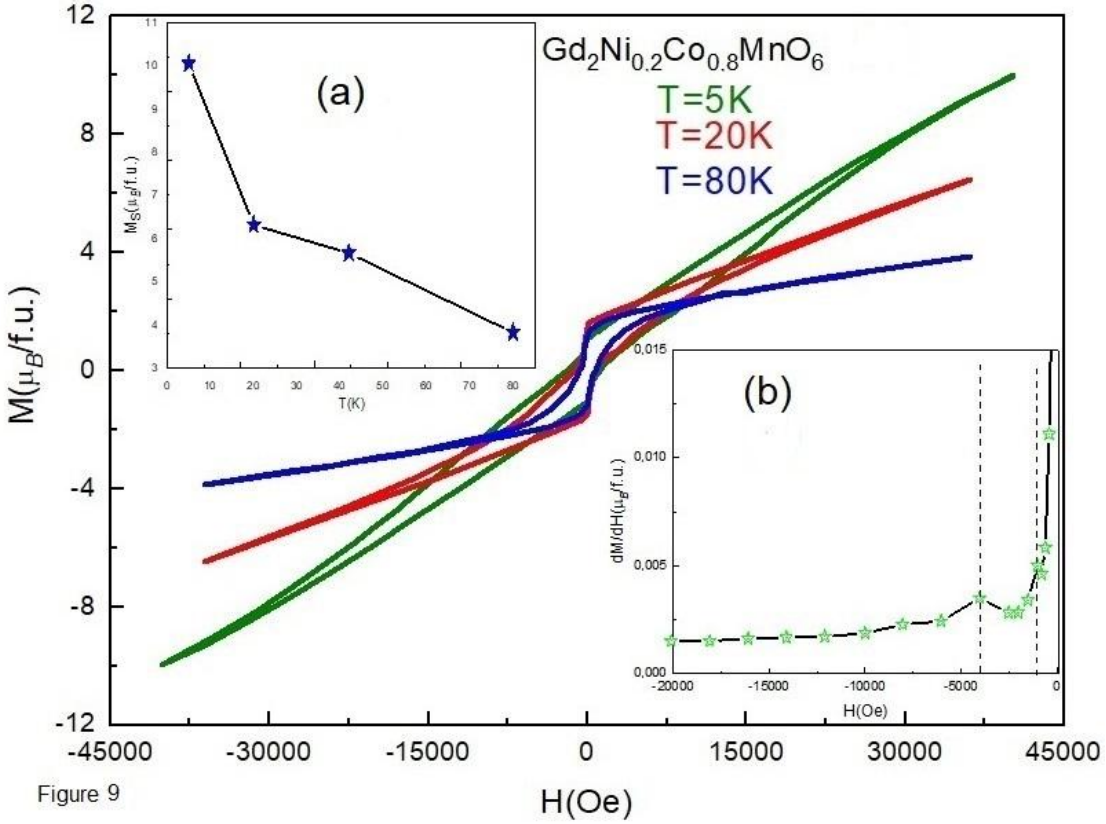
Gd2Ni0.2Co0.8MnO6
T=5K
T=20K
T=80K
(a)
(b)
M(μB/f.u.)
H(Oe)
MS(μB/f.u.)
T(K)
dM/dH(μB/f.u.)
H(Oe)

Figure 9

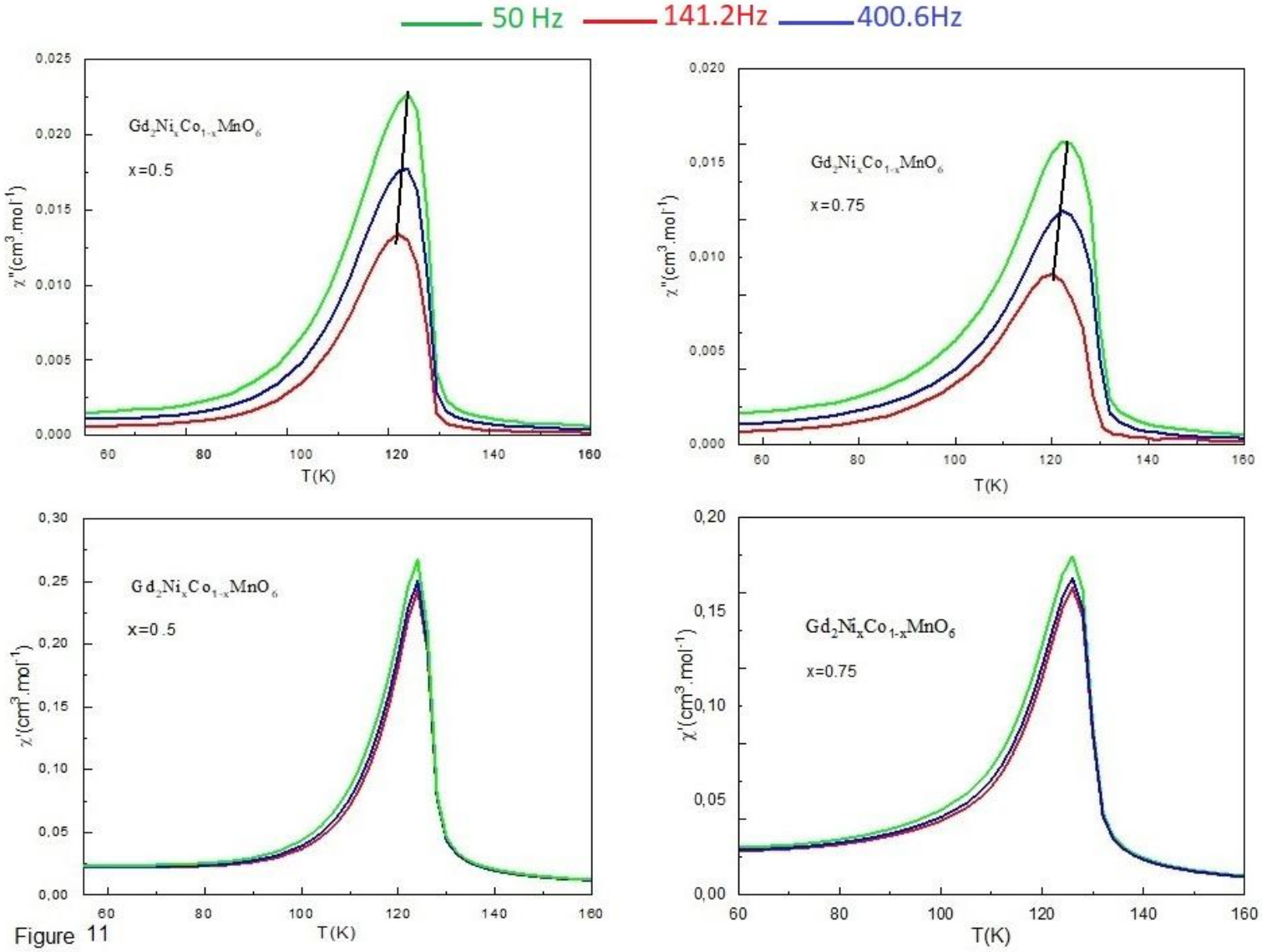
50 Hz
141.2Hz
400.6Hz
Gd2NixCo1-xMnO6
x=0.5
χ''(cm3.mol-1)
T(K)
Gd2NixCo1-xMnO6
x=0.75
χ''(cm3.mol-1)
T(K)
Gd2NixCo1-xMnO6
x=0.5
χ'(cm3.mol-1)
T(K)
Gd2NixCo1-xMnO6
x=0.75
χ'(cm3.mol-1)
T(K)

Figure 11

Table I

	x=0.2	x=0.25	x=0.5	x=0.75	x=0.8
a (Å)	5.30964	5.30464	2.0998	5.29670	5.2972
b (Å)	5.58187	5.57946	1.9275	5.55735	5.5500
c (Å)	7.55762	7.56555	2.5738	7.55961	7.5594
$\boldsymbol{\beta}^{\circ}$	90.04977	90.08794	145.61	90.04476	89.899
V $(Å)^3$	223.2524	223.9176	2.0998	222.1213	222.2419
χ^2	5.4	5.9	1.9275	7.4	4.7
Bond length and bond angles					
$< \mathbf{Ni/Co-O} >$ (Å)	2.1075	2.0998	2.0785	2.0827	2.0752
$< \mathbf{Mn-O} >$ (Å)	1.8928	1.9275	1.9321	1.9574	1.9443
$< \mathbf{Gd-O} > (Å)$	2.5328	2.5738	2.5240	2.5237	2.5291
<Mn-O-B>(°)	145.82	145.61	145.32	146.42	146.85

Table II

	Gd_2CoMnO_6		$Gd_2Ni_{0.5}Co_{0.5}MnO_6$		Gd_2NiMnO_6	
	Experimental	Theoretical	Experimental	Theoretical	Experimental	Theoretical
a (Å)	5.296	5.261	5.301	5.292	5.303	5.269
b (Å)	5.535	5.554	5.561	5.588	5.592	5.583
c (Å)	7.556	7.478	7.561	7.595	7.551	7.485

Table III

The gap energy (eV)	x=0	x=0.5	x=1
E_g (spin up ↑)	1.14	0.87	1.24
E_g(spin down↓)	2.34	2.33	2.93

Table IV

	x=0.2	x=0.25	x=0.5	x=0.75	x=0.8
T_{C1} (K)	121.90	123.73	124.33	127.12	128.63
T_{C2} (K)	-	-	116.43	-	136.75
T_N (K)	48.19	47.27	43.71	36.12	36.18
μ_{eff}-4f (μ_B)	12.75	11.63	11.38	11.14	10.96
μ_{eff}-3d (μ_B)	5.49	6.07	6.20	6.48	6.21
GP(%)	18.1	17.44	16.58	13.1	12.35
λ	0.752	0.764	0.706	0.68	0.63
$M_{s\ ext}$ (μ_B /f.u)	9.05	8.50	11.36	11.01	11.04
$M_{s0\ the}$ (μ_B /f.u)	19.80	19.75	19.50	19.25	19.20
$M_{s\ ext}/M_{s0\ the}$ (%)	45.70	43.03	58.25	57.19	57.5
M_r (μ_B /f.u)	1.13	1.16	1.38	1.08	1.02
H_c (Oe)	1335.08	167.22	1362.87	1245.80	1107.00

Captions

Figure.1. X-ray diffraction profiles of experimental (. . .) and calculated patterns (-----) for x=0.25. Inset (a) the lattice parameters as a function of Nickel content (x). Inset (b) show the monoclinic structure with $P2_1/n$ space group.

Figure.2. Raman spectra for the five oxides. Inset the energy of the phonons versus the nickel content x

Figure.3. The partial density of states (PDOS) and the calculated band structure of $Gd_2Ni_{0.5}Co_{0.5}MnO_6$ for spin up and spin down using (GGA+U) and (GGA) approximations.

Figure.4. $(\alpha hv)^2$ versus photon energy (hv) for $Gd_2Ni_xCo_{1-x}MnO_6$ (x = 0.25, 0.5) compounds.

Figure.5. Results from the M(T) measurements for the five oxides in the magnetic field of 50 Oe: thermal variation of ZFC-FC molar susceptibility (χ_M). Inset the curie-temperature T_C and Neel-temperature T_N as a function of the nickel content x.

Figure.6. Curve-fit to $\chi^{-1}(T)$ using a modified Curie–Weiss equation. Inset log10 $\chi^{-1}(T)$ versus log10(T-T_C^R) plots, the red solid lines represent the fit to the experimental data.

Figure.7. Evolution of Griffiths phase percentage (GP%) and value of λ as a function of the nickel content x.

$$\chi^{-1}(T) = A(T - T_C^R)^{1-\lambda}$$

Figure.8. field dependent magnetization for the five oxides at 43 K in the field range from -4 T to 4 T. Inset field dependent magnetization for the five oxides at 300 K in the field range from 0 to 7 T.

Figure.9. field dependent magnetization for $Gd_2Ni_xCo_{1-x}MnO_6$ (x = 2) at 5 K, 20 K, 43K and 80 K in the field range from -4 T to 4 T. Inset (a) the temperature dependence of M_s moments. Inset (b) the derivative of M(H) versus H at 20 K.

Figure.10. thermal variation of the real and imaginary molar susceptibilities (χ' and χ'') for x=0.5 and 0.75 oxides in an AC magnetic field of 3 Oe with three frequencies (50 Hz, 141.6 Hz and 400.6 Hz).

Table I. Structural parameters obtained by the Rietveld refinement of the X-ray diffraction pattern.

Table II. The band gap energy for $Gd_2Ni_xCo_{1-x}MnO_6$ (x = 0, 0.5, 1) using GGA+U approximation.

Table III. The calculated parameters for $Gd_2Ni_xCo_{1-x}MnO_6$ (x = 0, 0.5, 1) using Geometry optimization (BFGS) method.

Table IV. Magnetic parameters for $Gd_2Ni_xCo_{1-x}MnO_6$ double perovskites.

Highlights

- Tailoring Griffith-like phase cluster and spin glass formation with the chemical composition and temperature in double perovskite oxide manganese.
- Metamagnetic phase transition ascribed to the reorientation of Gd moments towards the Ni/Co/Mn sublattice.
- spin glass transition analog.